ISSN (Print) 1226-1750
ISSN (Online) 2233-6656
Journal of Magnetics 26(2), 199-204 (2021) https://doi.org/10.4283/JMAG.2021.26.2.199

PVP Encapsulated $Mn_{0.8}Zn_{0.2}Fe_2O_4$ Nanoparticles: Synthesis, Microstructure, and Magnetic Characterizations

Shanigaram Mallesh and Ki Hyeon Kim*

Department of Physics, Yeungnam University, Gyeongsan 38541, Republic of Korea

(Received 14 March 2021, Received in final form 13 April 2021, Accepted 13 April 2021)

We report the polyvinylpyrrolidone (PVP) encapsulated MnZn ferrite ($Mn_{0.8}Zn_{0.2}Fe_2O_4$/PVP) nanocomposite for low-temperature magnetic properties prepared by the facile one-pot sol-gel route. The transmission electron microscopy analysis revealed spherical shape ferrite particles in a polymer matrix ($Mn_{0.8}Zn_{0.2}Fe_2O_4$/PVP nanocomposite) with an average particle size of 11.6 nm. The Rietveld refinement of X-ray diffraction (XRD) data revealed the pure cubic spinel structure formation. The lattice parameter is 8.3825 Å, and the average crystallite size is 10 nm evaluated from XRD data. Raman spectroscopy analysis is in agreement with XRD results. The temperature-dependent magnetization analysis disclosed the effective anisotropy constant K_{eff}, the value of 3.0×10^4 J/m^3. The meticulous investigation of magnetic field-dependent magnetic properties from 2 K to 350 K unveiled superparamagnetic (SPM) behavior. From the electron spin resonance (ESR) analysis, the calculated g value and spin-spin relaxation time (T_2) are 2.03 and 2.52×10^{-11} sec, respectively, which confirms the SPM behavior.

Keywords : polyvinylpyrrolidone, $Mn_{0.8}Zn_{0.2}Fe_2O_4$/PVP nanocomposite, magnetization, coercivity, superparamagnetic

1. Introduction

Recently, the ferrite nanoparticles (NPs) have drawn much attention owing to their large surface-to-volume ratio and quantum confinement effect (shape and size-dependent properties) compared to their bulk counterparts [1]. These properties of NPs made them useful in several potential applications, including photocatalysts, sensors, electrochemical energy storage, electromagnetic, magnetic hyperthermia, and magnetic resonance imaging [1-4]. The physical/chemical properties of NPs are strongly dependent on composition and microstructure, which in turn dependent on synthesis methods and process conditions [1]. Several research groups have prepared MnZn ferrite NPs with various methods, including heat reflux [5], co-precipitation [6], solvothermal [7], and sol-gel [8]. The above-discussed reports examined the free-standing ferrite nanoparticles for microstructure and magnetic properties. However, free-standing/bare magnetic NPs are unstable, and they agglomerate together, which significantly degrade the magnetic properties. Therefore, stabilization and controlling the shape and size of the NPs with desired magnetic properties is highly challenging at the nanoscale level.

Polyvinylpyrrolidone (PVP), frequently used as a surfactant, can effectively regulate the nucleation and crystal growth of NPs and prohibit their particle agglomerations [9-11]. The PVP enables the thermal and chemical protection of NPs by forming a passive layer on the surface of magnetic NPs and enormously affects the physical and chemical properties of as-synthesized composites. Furthermore, PVP covering also affects their surface and interface properties [9-11]. Kashi *et al.* have investigated the structure and magnetic properties of $Co_xFe_{3-x}O_4$ (x = 0.5-2.0) NPs in the PVP matrix prepared by the hydrothermal method [12]. A considerable variation in magnetization and coercivity was observed with PVP concentration. Jalalian *et al.* designed cobalt ferrite NPs using PVP as a surfactant by a hydrothermal method. They have observed that the microstructure and magnetic properties are strongly influenced by the increased PVP content [13]. Seo *et al.* examined the effect of PVP on the formation of iron oxide NPs in a polyol synthesis technique. The PVP protected the NPs from oxidation and significantly reduced the size compared to bare iron oxide NPs [14].

Herein, we prepared the $Mn_{0.8}Zn_{0.2}Fe_2O_4$/PVP nano-

*Corresponding author: Tel: +82-53-810-2334
Fax: +82-53-810-4616, e-mail: kee1@ynu.ac.kr

composite by a facile single-step sol-gel process. The microstructure, particle size distribution, and vibrational properties have been investigated using XRD, TEM, and Raman spectra. The average blocking temperature (T_B) and anisotropy constant were evaluated from the temperature-dependent magnetization data. The M-H curves are measured below and above T_B to understand the origin of the ground state of magnetic behavior. The remanent magnetization and coercivity decreased with the increase of temperature up to T_B and became negligible above the T_B. Further, magnetic interactions (magnetic resonance field, g-value, and T_2) were analyzed using ESR spectra.

2. Experimental details

High purity of $Mn(NO_3)_2{\cdot}4H_2O$, $Zn(CH_3COO)_2{\cdot}2H_2O$, $Fe(NO_3)_3{\cdot}9H_2O$, and polyvinylpyrrolidone (PVP) precursors were used as received without further purification. The PVP capsulated MnZn ferrite ($Mn_{0.8}Zn_{0.2}Fe_2O_4$/PVP) nanocomposite prepared by the simple one-pot sol-gel technique based on earlier work [8]. The stoichiometric amounts of nitrate salts were dissolved in ethylene glycol, and then glycerol was inserted to stabilize the solution under continuous magnetic stirring at 80 °C for 30 minutes. Further, the PVP was added to the above solution under continuous magnetic stirring for another 20 minutes. After that, the above solution was allowed to cool down to room temperature. Additionally, 2-propanol and triethylamine were mixed with the solution under constant stirring for 10 minutes at room temperature. Finally, the solution gradually turned into a thick brown gel, then stirring was stopped, and the gel was slowly heated to 200 ºC and kept for 5 hours to obtain the $Mn_{0.8}Zn_{0.2}Fe_2O_4$/PVP nanocomposite.

The X-ray diffraction (XRD) results were obtained with PANalytical (X'pert PRO, CuKα (λ = 1.54059 Å). Vibrational properties were examined using Raman spectra (Jobin-Yvon LabRAM HR800UV). The microstructure and morphology of the as-prepared material were analyzed with transmission electron microscopy (TEM) using TECNAI-30 G_2 S-Twin. The temperature and magnetic field-dependent magnetization characteristics were carried out using a superconducting quantum interference device vibrating sample magnetometer (SQUID VSM, Quantum Design). The electron spin resonance (ESR) spectrum was measured using a JEOL-JES-FA200 X-band (9.455 GHz) spectrometer.

3. Results and Discussions

Figure 1(a, b) shows the TEM images of $Mn_{0.8}Zn_{0.2}Fe_2O_4$/PVP nanocomposite at different magnifications. The PVP encapsulated ferrite NPs exhibited a spherical shape with nanocrystalline nature. The particle size distribution obtained by measuring the sizes of 100 particles and the average particle size is 11.7 nm, which is evaluated from the size distribution histogram, as displayed in Fig. 1(c). The selected area electron diffraction (SAED) pattern revealed the concentric ring patterns, as shown in Fig. 1(d), which further suggests the nanocrystalline nature of the sample. The rings labeled in the SAED pattern correspond to the different lattice planes and are identical to

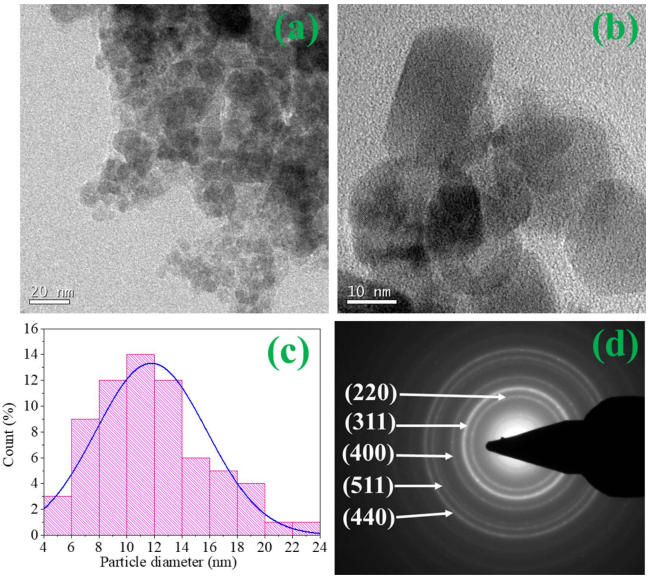

Fig. 1. (Color online) (a-d) TEM images, size distribution histogram, and SAED pattern of as-prepared $Mn_{0.8}Zn_{0.2}Fe_2O_4$/PVP nanocomposite.

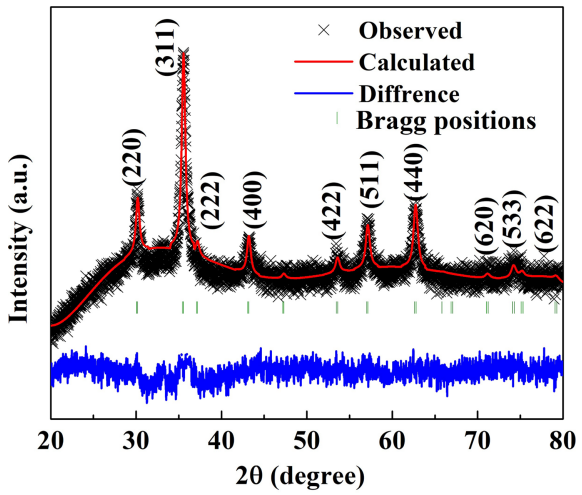

Fig. 2. (Color online) XRD patterns of as-prepared $Mn_{0.8}Zn_{0.2}Fe_2O_4$/PVP nanocomposite.

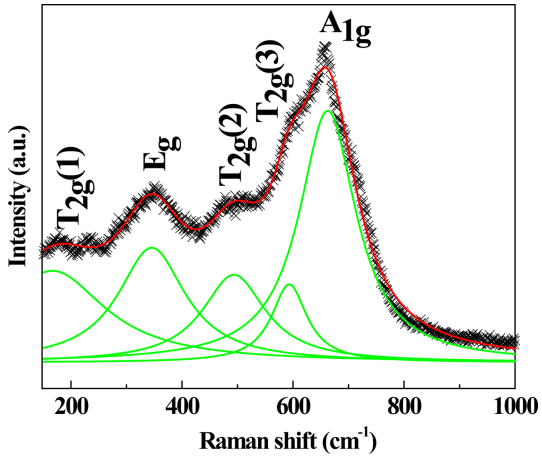

Fig. 3. (Color online) Raman spectra of as-prepared $Mn_{0.8}Zn_{0.2}Fe_2O_4$/PVP nanocomposite.

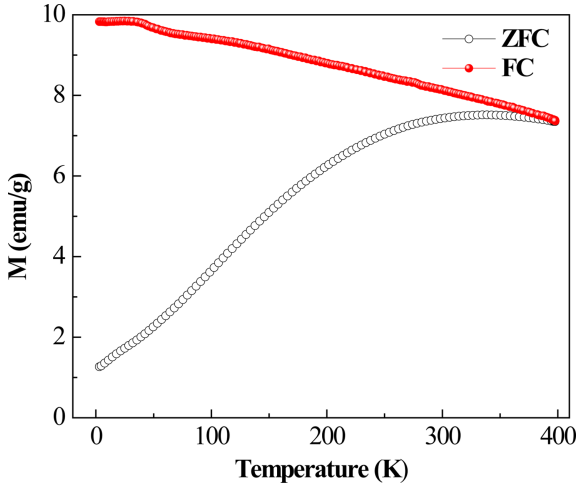

Fig. 4. (Color online) ZFC-FC magnetization of as-prepared $Mn_{0.8}Zn_{0.2}Fe_2O_4$/PVP nanocomposite.

the single-phase cubic spinel structure [18].

Figure 2 demonstrates the Rietveld refinement of the X-ray diffraction (XRD) pattern of $Mn_{0.8}Zn_{0.2}Fe_2O_4$/PVP nanocomposite. The refinement result to all diffraction peaks confirms the cubic spinel structure of $Mn_{0.8}Zn_{0.2}Fe_2O_4$ NPs. The evaluated lattice parameter (a) is 8.3825 Å, and bond lengths of A, B sites are 1.69 nm (M_A-O) and 2.17 nm (M_B-O), respectively. The broadening of the diffraction peaks indicates the nanocrystalline nature of the particles. Therefore, the average crystallite size is determined to be 10 nm for $Mn_{0.8}Zn_{0.2}Fe_2O_4$ NPs in a PVP matrix.

Figure 3 presents the Lorentzian fit to the Raman spectra of $Mn_{0.8}Zn_{0.2}Fe_2O_4$/PVP nanocomposite obtained at room temperature in the frequency range of 100-1000 cm^{-1}. Generally, cubic spinel structures display five Raman active modes (A_{1g}+E_g+3T_{2g}) in ambient conditions [16]. The A_{1g} mode observed around 663 cm^{-1}, which is due to the symmetric stretching of oxygen ions at tetrahedra AO_4. The E_g and T_{2g}(3) modes detected at 334 cm^{-1} and 593 cm^{-1} and assigned to the symmetric and asymmetric bending of oxygen ions concerning the metal cations (Fe/Mn/Zn). T_{2g}(2) mode observed at 492 cm^{-1}, which is because of asymmetric stretching of Fe, and O. The T_{2g}(1) mode is observed at 163 cm^{-1} due to the complete translatory motion of FeO_4 [8]. Therefore, the manifestation of five Raman modes further confirms the cubic spinel structure of the $Mn_{0.8}Zn_{0.2}Fe_2O_4$ NPs in a polymer matrix. Raman outcomes are in agreement with XRD and TEM studies.

Figure 4 presents the zero-field-cooled (ZFC) and field-cooled (FC) magnetization of $Mn_{0.8}Zn_{0.2}Fe_2O_4$/PVP nanocomposite measured as a function of temperature under the field of 100 Oe. The magnetization increases with decreasing temperature in the ZFC curve and reached a broad maximum at a characteristic temperature (T_{max}). The broad peak is due to the size distribution of NPs, as evidenced from TEM (Fig. 1). Further, the ZFC and FC magnetization curves bifurcated above T_{max}. The average blocking temperature can be evaluated from the ZFC magnetization curve using the following relation:

$$\langle T_B \rangle = T_{max}/\beta \quad (1)$$

The typical range of β varied from 1.5 to 2 for SPM systems [17]. The β value changes significantly based on the interactions present in the system. The β value of densely packed SPM NPs is observed below 1.5. In this current study, we used a value of β = 1.7 by considering nearly non-interacting (SPM) particles. Therefore, using the T_{max} = 346 ± 3 K (which is attained from M-T the curve), the obtained value of $\langle T_B \rangle$ is 203 ± 3 K. Further, using $\langle T_B \rangle$ the effective magnetic anisotropy (K_{eff}) is evaluated using Eq. (2) [17, 18]

$$K_{eff} = 25\ k_B T_B / V \quad (2)$$

where, k_B is the Boltzmann constant (1.38×10^{-23} $J \cdot K^{-1}$) and V is the average volume of the particles obtained from TEM. Thus, the value of effective magnetic anisotropy is 3.0×10^4 J/m^3. This value is in agreement with earlier reports on ferrite NPs [17]. Therefore, the magnetic NPs exhibit SPM relaxation when thermal energy overcomes the anisotropy energy barrier.

Figure 5 displays the magnetic field-dependent magnetization of the $Mn_{0.8}Zn_{0.2}Fe_2O_4$/PVP nanocomposite at different temperatures (5 K-350 K). From the M-H curves, the following notes made that; (i) the magnetization of the NPs does not saturate up to an applied field of 60 k Oe,

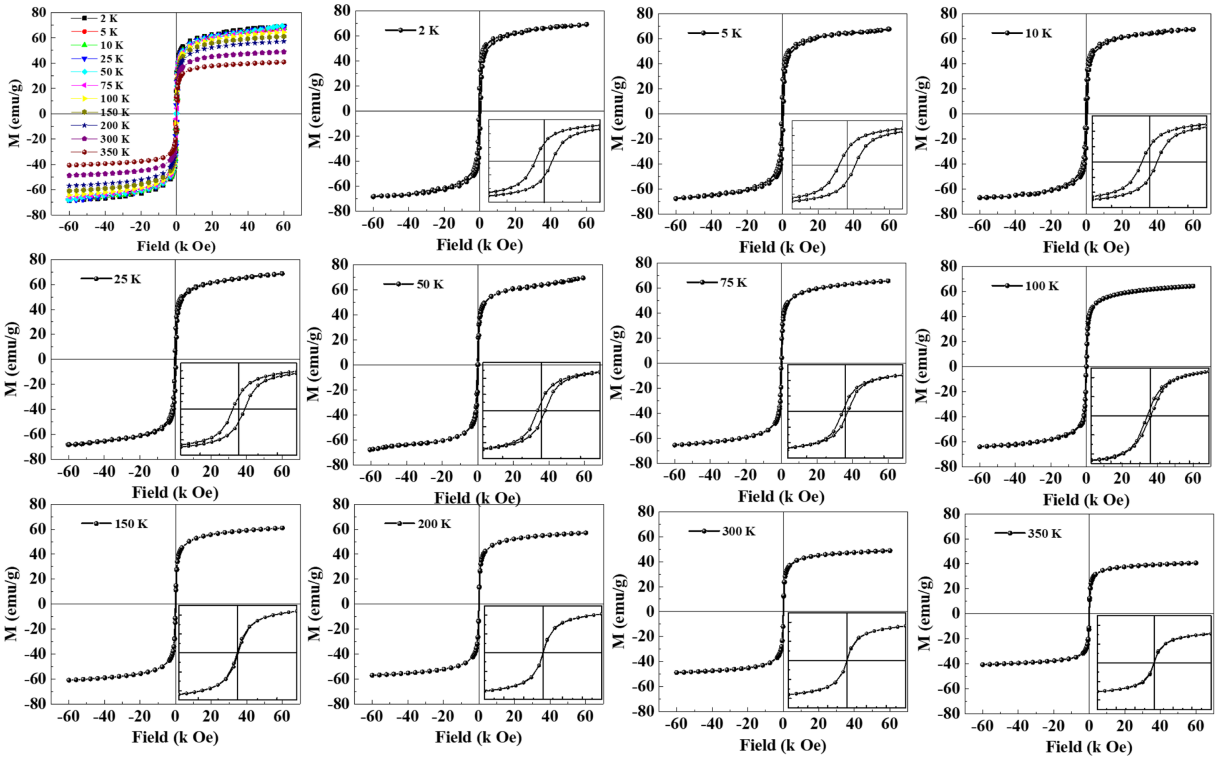

Fig. 5. (Color online) M-H curves measured at various temperatures for as-prepared $Mn_{0.8}Zn_{0.2}Fe_2O_4$/PVP nanocomposite.

which might be due to the existence of strain and surface defects in the NPs. Similar behavior was observed in an earlier report on PVP/$MnFe_2O_4$ nanocomposite [11]. (ii) M-H curves at low fields exhibit symmetric hysteresis loop with a high coercivity (H_C) ~10^2 Oe below T_{max}; negligible H_C and remanent magnetization (M_R) observed above T_{max}. Below the blocking temperature, the anisotropy energy much larger than the thermal energy (KV >> k_BT_B). Hence the single domains are stable and exhibit a hysteresis loop. Above the blocking temperature, the thermal energy is much larger than the anisotropy energy (KV << k_BT_B), where the single domains are unstable, which leads to SPM behavior. To further analyze the magnetic character, M (obtained at 60 kOe), M_R and H_C received from the M-H curves are plotted as a function of temperature for $Mn_{0.8}Zn_{0.2}Fe_2O_4$/PVP nanocomposite, as shown in Fig. 6. The value of M is 69.5 emu/g at 2 K, which decreases monotonously with the increase of temperature and reaches a value of 41.2 emu/g at 350 K. The obtained M values are lower than the value of bulk $Mn_{0.8}Zn_{0.2}Fe_2O_4$ (90 emu/g) [8]. However, the $Mn_{0.8}Zn_{0.2}Fe_2O_4$/PVP nanocomposite's magnetization value is considerably larger than the PVP/$MnFe_2O_4$ nanocomposite [11]. The value of M decreases from 52.1 emu/g to 40.4 emu/g as the temperature increases from 10 K to 300 K for PVP/$MnFe_2O_4$ nanocomposite [11]. The enhanced magnetization in $Mn_{0.8}Zn_{0.2}Fe_2O_4$/PVP nanocomposite compared to PVP/$MnFe_2O_4$ nanocomposite is attributed to the presence of nonmagnetic Zn^{2+} ions, which can increase the uncompensated magnetic moment between tetrahedral and octahedral sites [8]. The increase of thermal agitations supports the unstable single domain particle nature. For the NPs below the SPM size limit (< 20 nm for ferrites), thermal energy suppresses the anisotropy energy and hence causes SPM relaxation in NPs [8, 19]. The average particle size of $Mn_{0.8}Zn_{0.2}Fe_2O_4$/PVP nanocomposite is 11.6 (TEM) within the SPM limit. The H_C is 460 Oe at 2 K, which drastically decreases with increased temperature and becomes negligible above the T_B. To further investigate this behavior, the H_C is articulated by Kneller's law [20]

$$H_C(T) = H_C(0)\left[1-\left(\frac{T}{T_B}\right)^{1/2}\right] \quad (3)$$

where $H_C(0)$ is the maximum coercive field at T = 0 K and H_C = 0 at $T = T_B$. Therefore, the linear relation between the H_C and $T^{1/2}$, as shown in the inset of Fig. 6(c), supports a non-interacting system with SPM relaxation [15].

The X-band ESR spectrum was recorded at room temperature for as-prepared $Mn_{0.8}Zn_{0.2}Fe_2O_4$/PVP nano-

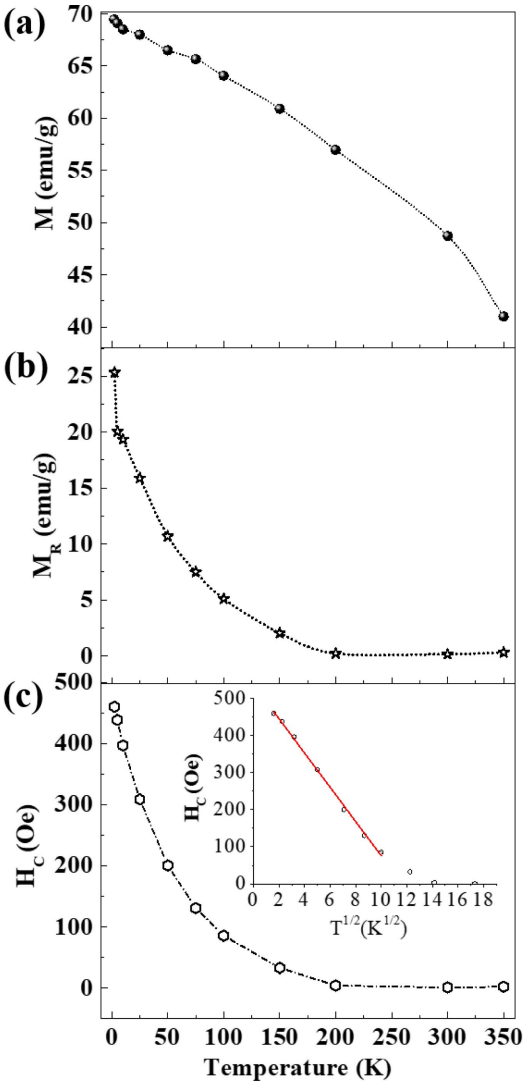

Fig. 6. (Color online) Magnetization, remanent magnetization, and coercivity as a function of temperature for as-prepared $Mn_{0.8}Zn_{0.2}Fe_2O_4$/PVP nanocomposite.

composite to understand the magnetic interactions. The peak-to-peak line-width (ΔH_{pp}), magnetic resonance field (H_r), g-factor, and spin-spin relaxation time (T_2) are the essential parameters to analyze the magnetic interactions present in the system. From the ESR signal, the g-value can be estimated by $\Delta E = hf = g\mu_B H_r$, where h is the Planck constant, f is the microwave frequency, μ_B is Bohr magneton, and H_r (276 mT) is the magnetic resonance field at which resonance arises [21, 22]. The obtained value of g for SPM particles is 2.03, which is in good agreement with earlier reports [21, 22]. The spin relaxation procedure is described by a time constant, which relies on the rate of microwave energy absorption or dissipation in the presence of the static magnetic field. Therefore, the T_2 is the energy difference (ΔE) transported

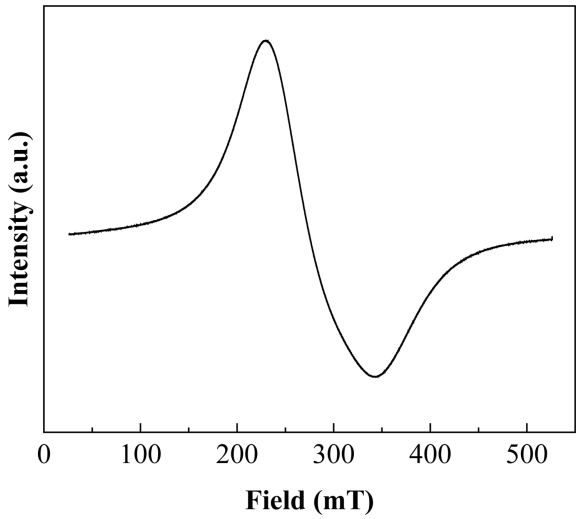

Fig. 7. ESR spectra of as-prepared $Mn_{0.8}Zn_{0.2}Fe_2O_4$/PVP nanocomposite.

to adjacent electrons, which can be evaluated using the peak-to-peak line-width as following;

$$\frac{1}{T_2} = \frac{g\mu_B \Delta H_{1/2}}{\hbar}, \ \Delta H_{1/2} = \sqrt{3}\ \Delta H_{pp} \quad (4)$$

where μ_B is the Bohr magneton (9.274×10^{-21} erg G^{-1}) and $\hbar$ is a Planck constant (1.05×10^{-27} erg s) [23]. The estimated value of the T_2 is 2.52×10^{-11} sec for a given ΔH_{pp} = 111 mT. This value is in good agreement with SPM particles [21, 22]. The detailed analysis of the microstructure and magnetic studies confirmed the SPM behavior. Therefore, the $Mn_{0.8}Zn_{0.2}Fe_2O_4$/PVP nanocomposite material can be helpful for magnetic hyperthermia applications.

4. Conclusions

We have investigated the microstructure and magnetic properties of PVP encapsulated $Mn_{0.8}Zn_{0.2}Fe_2O_4$ NPs synthesized by a simple one-pot sol-gel process. The TEM analysis revealed the formation of PVP capped ferrites (11.6 nm) NPs ($Mn_{0.8}Zn_{0.2}Fe_2O_4$/PVP) nanocomposite. The cubic spinel structure construction is confirmed from the TEM, XRD, and Raman analyses. The average blocking temperature is T_B = 216 ± 3 K), and the effective anisotropy constant K_{eff} is 3.0×10^4 J/m^3 evaluated using temperature-dependent magnetization data. Magnetization of the sample is decreased with the increase of measuring temperature. The magnetic characters (negligible M_R and H_C above the T_B) and ESR parameters (g = 2.03 and $T_2 = 2.52 \times 10^{-11}$ sec) further confirmed the SPM behavior.

Acknowledgment

This research was supported by Creative Materials Discovery Program through the National Research Foundation of Korea (NRF) funded by Ministry of Science and ICT (2020M3D1A2080950).

References

[1] J. Xie, C. Yan, Y. Zhang, and N. Gu, Chem. Mater. **25**, 3702 (2013).
[2] P. Thakur, D. Chahar, S. Taneja, N. Bhalla, and A. Thakur, Ceram. Int. **46**, 15740 (2020).
[3] S. Mallesh, W. Jang, and K. H. Kim, Phys. Lett. A **389**, 127069 (2021).
[4] Z. Zhao, Z. Zhou, J. Bao, Z. Wang, J. Hu, X. Chi, K. Ni, R. Wang, X. Chen, Z. Chen, and J. Gao, Nat. Commun. **4**, 2266 (2013).
[5] J. Park, K. An, Y. Hwang, J.-G. Park, H.-J. Noh, J.-Y. Kim, J.-H. Park, N.-M. Hwang, and T. Hyeon, Nat. Mater. **3**, 891 (2004).
[6] Y. Liu and J. Hsu, Appl. Sci. **8**, 1005 (2018).
[7] S. Bai, X. Shen, X. Zhong, Y. Liu, G. Zhu, X. Xu, and K. Chen, Carbon **50**, 2337 (2012).
[8] S. Mallesh and V. Srinivas, J. Magn. Magn. Mater. **475**, 290 (2019).
[9] T. Zhu, S. Changa, Y.-F. Songa, M. Lahoubic, and W. Wang, Chem. Eng. J. **373**, 755 (2019).
[10] K. M. Koczkur, S. Mourdikoudis, L. Polavarapu, and S. E. Skrabalak, Dalton Trans. **44**, 17883 (2015).
[11] R. Topkaya, U. Kurtan, A. Baykal, and M. S. Toprak, Ceram. Inter. **39**, 5651 (2013).
[12] M. A. Kashi, S. A. Arani, E. B. Jebeli, and A. H. Montazer, Appl. Phys. A **126**, 250 (2020).
[13] M. Jalalian, S. M. Mirkazemi, and S. Alamolhoda, Appl. Phys. A **122**, 835 (2016).
[14] K. Seo, K. Sinha, E. Novitskya, and O. A. Graeve, Mater. Lett. **215**, 203 (2018).
[15] S. Mallesh, V. Srinivas, M. Vasundhara, and K. H. Kim, Physica B **582**, 411963 (2020).
[16] J. L. Verble, Phys. Rev. B **9**, 5236 (1974).
[17] S. Morup, F. Bodker, P. V. Hendriksen, and S. Linderoth, Phys. Rev. B **52**, 287 (1995).
[18] M. Respaud, J. M. Broto, H. Rakoto, A. R. Fert, L. Thomas, B. Barbara, M. Verelst, E. Snoeck, P. Lecante, A. Mosset, J. Osuna, T. Ould Ely, C. Amiens, and B. Chaudret, Phys. Rev. B. **57**, 2925 (1998).
[19] K. Mandal, S. Chakraverthy, S.P. Mandal, P. Agudo, M. Pal, and D. Chakravorthy, J. Appl. Phys. **92**, 501 (2002).
[20] E. F. Kneller and F. E. Luborsky, J. Appl. Phys. **34**, 656 (1963).
[21] S. Sui, D. P. Xu, F. L. Zheng, and W. H. Su, J. Appl. Phys. **80**, 719 (1996).
[22] N. E. Domracheva, A. V. Pyataev, R. A. Manapov, and M. S. Gruzdev, Chem. Phys. Chem. **12**, 3009 (2011).
[23] G. Dixit, J. P. Singh, R. C. Srivastava, and H. M Agrawal, J. Magn. Magn. Mater. **324**, 479 (2012).